Power uprates
and plant life extension

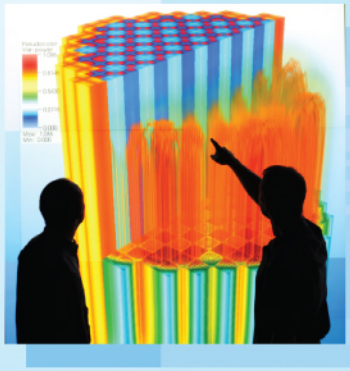

Engineering design
and analysis

Science-enabling
high performance
computing

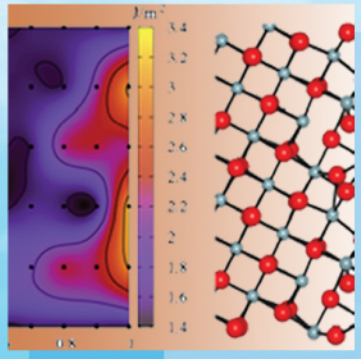

Fundamental science

Plant operational data

CASL-U-2011-0185-000

Consortium for Advanced Simulation of LWRs

ITM Benchmark #1: PHASTA Results

Igor Bolotnov

North Carolina State University

September 30, 2011

U.S. DEPARTMENT OF ENERGY | Nuclear Energy

ITM Benchmark #1: PHASTA results

L3:THM.ITM.P3.02 milestone report

Igor Bolotnov, North Carolina State University

September 2011

CASL-U-2011-0185-000

Table of Contents

List of Figures 3
List of Tables 4
Introduction and Background 5
PHASTA Overview 5
Cases Overview 6
Smooth wall 6
Square rod roughened wall 7
Rough wall channel with hemispherical obstacles 8
Results 11
Data acquisition and analysis 11
Smooth wall 11
Square rod roughened wall 13
Rough wall channel with hemispherical obstacles 18
PHASTA **strong** scaling study 22
PHASTA **weak** scaling study 24
Computational cost summary 25
Conclusions and Future Work 25
References 26

List of Figures

Figure 1. Simulation domain dimensions and axis orientation. Walls are shown as shaded areas. 6
Figure 2. Part of the simulation domain for smooth wall case. 7
Figure 3. Typical velocity distribution in the rectangular roughness turbulent channel flow. 8
Figure 4. Detailed view of one roughness element with domain grid (the grid is hexahedral, visualization software shows the triangles). 8
Figure 5. Law of the wall comparison between standard and reduced-size domains with smooth walls. 9
Figure 6. Typical velocity distribution in the hemispherical roughness turbulent channel flow. 10
Figure 7. Detailed view of hemispherical roughness elements with computational grid (size view on the left and top view on the right). Blocked regions shown in blue. 10
Figure 8. Overview of hemispherical roughness elements. 10
Figure 9. Mean velocity (red line) and turbulent kinetic energy (purple line) profiles for smooth channel flow simulation. 12
Figure 10. Smooth wall channel flow compared with the law of the wall. PHASTA (circles) and TransAT LES (Chatzikyriakou, et al., 2011a) (triangles) results are shown. 12
Figure 11. Comparison of mean velocity and turbulent kinetic energy profiles at measurement station 2 averaged at two consecutive time windows to ensure the code statistical convergence for rectangular roughness case. Latest time window is shown with dashed lines. 13
Figure 12. Measuring station locations with respect to rectangular roughness elements (Ashrafian, et al., 2004). 14
Figure 13. PHASTA results of inner scaling mean velocity profiles at 4 stations shown in Figure 12. . 14
Figure 14. Mean velocity (triangles) profiles at $x/\lambda = 0.312$ obtained by (Ashrafian, et al., 2004). Circles show smooth channel data by (Moser, et al., 1999). (a) outer scaling; (b) defect law, inner scaling; (c) defect law, outer scaling and (d) inner scaling. Figure is scanned from (Ashrafian, et al., 2004). 15
Figure 15. PHASTA mean velocity profiles at $x/\lambda = 0.312$ for smooth channel (circles) and rectangular roughness wall channel (triangles). The plots are the same as in Figure 14. 16
Figure 16. Mean velocity profiles in inner coordinates for smooth and rough (rectangular roughness elements) channel flow simulations by PHASTA (violet and blue solid lines) and DNS results by (Krogstad, et al., 2005) (symbols). TransAT/MIT result is shown in red (Chatzikyriakou, et al., 2011a). 16
Figure 17. Reynolds stresses in inner coordinates, normalized by u_τ^2. Solid black line shows the height of roughness elements, black dashed line designates roughness sublayer. Colors designate Reynolds stress component: $\langle u'^2 \rangle$ is red; $\langle v'^2 \rangle$ is green; $\langle w'^2 \rangle$ is blue; $\langle u'v' \rangle$ is violet. Line style shows the measuring station location: Station 1: dashed lines; Station 2: dash-dot lines; Station 3: dash-dot-dot lines; Station 4: dotted lines. 17
Figure 18. Reynolds stresses in inner coordinates, normalized by u_τ^2. The legend is the same as in Figure 17. 18
Figure 19. Comparison of mean velocity and turbulent kinetic energy profiles at measurement station 2 averaged at two consecutive time windows to ensure the code statistical convergence for hemispherical roughness case. 18
Figure 20. Location of 7 virtual probe sets in the hemispherical roughness case. 19

Figure 21. Mean velocity profiles at different measuring stations compared with the smooth wall result and the law of the wall plots. Dotted line shows TransAT LES (Chatzikyriakou, et al., 2011a). 19
Figure 22. Reynolds stresses in inner coordinates, normalized by u_τ^2. Solid black line shows the height of roughness elements, black dashed line designates roughness sublayer. Each plot shows one component for all 7 measuring stations. Coloring is consistent with Figure 21..... 20
Figure 23. Comparison of velocity magnitude structure in planes, parallel to the wall at various y^+ locations. Smooth wall solution is shown on the left and rough wall with hemispheres on the right. 21
Figure 24. Cross-section of large bubble simulation domain with velocity distribution shown in color, interface (white line) and level set distance field contour (black lines). 23
Figure 25. Wall clock time vs. Number of cores. 10 iteration times are shown in seconds..... 24
Figure 26. Total time to ideal time ratio. Perfect scaling would mean a horizontal line at 100%. 24

List of Tables

Table 1. Smooth wall simulation mesh parameters..... 7
Table 2. Rectangular roughness wall simulation mesh parameters 8
Table 3. Hemispherical roughness wall simulation mesh parameters..... 9
Table 4. Gas/Liquid properties in the simulation: 22
Table 5. Summary of PHASTA strong scaling study 23
Table 6. Weak scaling study domain parameters (Re_τ = 400) 25
Table 7. Weak scaling PHASTA performance 25

Introduction and Background

A set of benchmark cases has been defined by CASL-THM members to evaluate the performance of various codes with interfacial tracking (ITM) capabilities. The first ITM benchmark (Chatzikyriakou, et al., 2011b) tests single-phase adiabatic turbulence modeling in a channel with smooth and rough walls.

PHASTA code was previously validated (Trofimova, et al., 2009) for a smooth wall channel case against theoretical knowledge (such as law of the wall) and available experimental and numerical data (Moser, et al., 1999). The present study will test PHASTA's capabilities for smooth and rough wall channel flows. The following cases are simulated using ORNL leadership computing facility (Jaguar, 2011):

- smooth wall turbulent channel flow, validated (Moser, et al., 1999)
- roughened wall with square rods, validated (Ashrafian, et al., 2004), (Krogstad, et al., 2005)
- roughened wall with hemispherical solid obstacles (Chatzikyriakou, et al., 2011b), a database was generated for validation of other non-DNS codes (RaNS, LES)

Recent results (Bolotnov, et al., 2011) show that PHASTA is capable of predicting both single and two-phase flows and the present report will describe the results of the test cases performed to satisfy the requirements of the ITM benchmark case #1.

PHASTA Overview

PHASTA is a parallel, hierarchic, higher-order accurate (from the 2nd to the 5th order accuracy, depending on function choice), adaptive, stabilized (finite element) transient analysis flow solver (both incompressible and compressible). This approach has been shown by (Jansen, 1999) and (Whiting & Jansen, 2001) to be an effective tool for bridging a broad range of length scales in turbulent (RANS, large-eddy simulation (LES), detached eddy simulation (DES), DNS) flows. PHASTA (and its predecessor, ENSA) was the first unstructured grid LES code (Jansen, 1993) and has been applied to turbulent flows ranging from validation benchmarks (channel flow, decay of isotropic turbulence) to complex flows (airfoils at maximum lift, flow over a cavity, near lip jet engine flows and fin-tube heat exchangers). The PHASTA code uses advanced anisotropic adaptive algorithms (Sahni, et al., 2006) and the most advanced LES/DES models (Tejada-Martinez & Jansen, 2005). Note that DES, LES, and DNS are computationally intensive even for single phase flows. This capability has been recently (Nagrath, et al., 2006) extended to two phase flows where we use the level set method to track the boundary between two immiscible fluids (either compressible - where we captured new instabilities in sonoluminescence, or incompressible – to study bubble coalescence and two-phase turbulence (Bolotnov, et al., 2011)). PHASTA uses anisotropically adapted unstructured grids and its highly scalable performance on massively parallel computers has already been demonstrated (the code has shown good scaling out to 288*1024 IBM Blue Gene processors, at JUGENE, BG/P (Germany, #12 in top500 as of June 2011)), (Zhou, et al., 2010).

PHASTA is an *open source* code. However, in the current setup, it uses commercial linear solver libraries from Acusim, Inc. A possible switch to open-source solvers is considered (e.g. Trilinos, PETSc). Meshing capabilities utilize tools from Simmetrix, Inc. Creating mesh converters from open-source tools to PHASTA format is also a possibility. PHASTA works with hexahedral, tetrahedral and mixed meshes.

Cases Overview

Even though all the cases under consideration have the same basic geometry (flow between parallel plates) they have different meshing requirements due to various wall roughness features.

Smooth wall

For a smooth wall direct numerical simulation (DNS) we aim to resolve the turbulence fluctuations down to Kolmogorov's scale. Typically mesh resolution is expressed in terms of viscous units, which are defined as:

$$\Delta x_i^+ = \frac{u_\tau \Delta x}{\nu} \tag{1}$$

where ν is the kinematic viscosity, u_τ is the friction velocity:

$$u_\tau = \sqrt{\frac{\tau_w}{\rho}} \tag{2}$$

Here τ_w is the wall shear stress and ρ is the fluid density. Table 1 summarizes the channel flow domain parameters. Note that the normal to the wall resolution (y) is variable to properly resolve viscous sublayer. The mesh size used for smooth wall simulation is 9.29 million hexahedral elements.

Figure 1 shows a basic schematic of the computational domain. Periodic boundary conditions are applied in x (stream-wise) and z (span-wise) directions. No-slip boundary condition is applied at the walls.

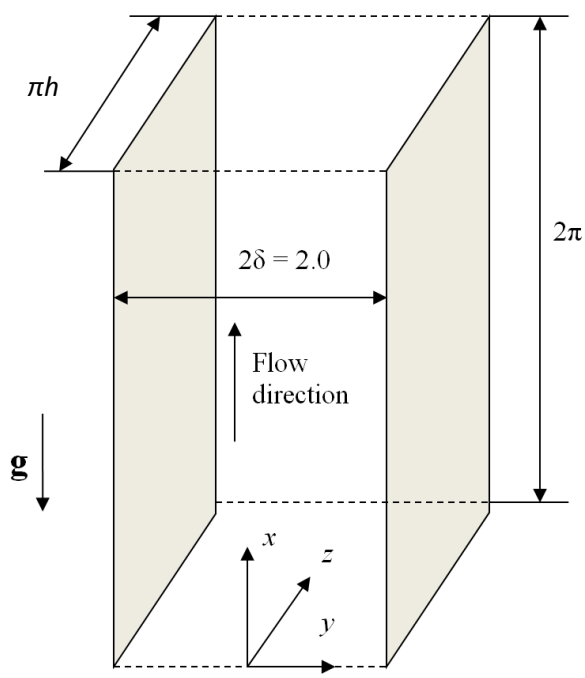

Figure 1. Simulation domain dimensions and axis orientation. Walls are shown as shaded areas.

Table 1. Smooth wall simulation mesh parameters

Direction:	Boundaries:	Number of nodes:	Resolution:
x	0.0 … 2πh	256	$\Delta x^+ = 9.8$
y	-1.0h … 1.0h	189	$\Delta y^+ = 0.5 \ldots 5.0$
z	0.0 … πh	192	$\Delta z^+ = 6.5$

Figure 2 shows the hexahedral mesh structure designed for the smooth wall simulation.

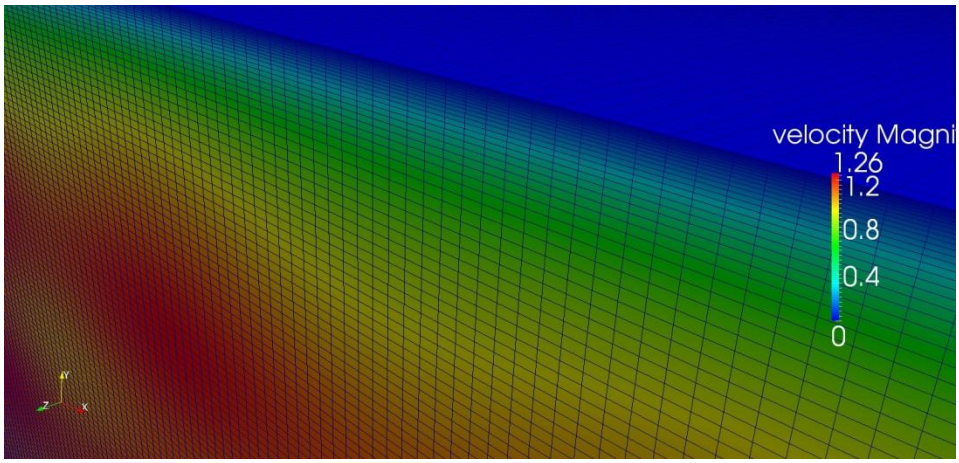

Figure 2. Part of the simulation domain for smooth wall case.

Square rod roughened wall

The second case was developed to validate PHASTA abilities in performing DNS of rough wall flows. The wall roughness was designed the same way as in DNS results of (Ashrafian, et al., 2004) and corresponding experimental study of (Krogstad, et al., 2005).

The challenge in simulating turbulent flows with rough walls is not only in resolving fine turbulent structures, but also adequately representing individual obstacles which collectively make up the rough wall.

Finite-element approach used in PHASTA allows application of no-slip condition to any internal node in the domain (the fluid velocity at a chosen set of nodes can be set to zero). While this would allow representing the roughness without a major re-design of the domain, care should be exercised to ensure the proper resolution of the individual roughness elements.

We used square rod roughness parameters according to the description provided in (Ashrafian, et al., 2004):

- square height/width: $k = 0.034h$
- stream-wise distance between the roughness elements: $\lambda = 8k = 0.272h$

In order to properly apply periodic boundary conditions in the stream-wise direction, the domain length has to be revised. Also, since the no-slip condition was applied to represent the roughness elements, mesh resolution has to be revised as well. Table 2 presents a summary of the computational domain parameters. The mesh size used in the simulation is 22M hexahedral elements.

Table 2. Rectangular roughness wall simulation mesh parameters

Direction:	Boundaries:	Number of nodes:	Resolution:
x	0.0 … 6.528h	768	$\Delta x^+ = 3.4$
y	-1.0h … 1.0h	179	$\Delta y^+ = 0.5 \ldots 6.5$
z	0.0 … πh	160	$\Delta z^+ = 7.8$

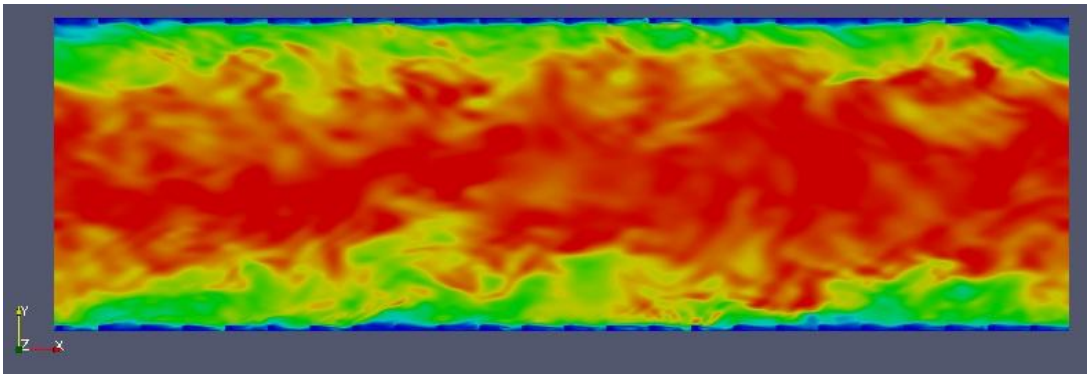

Figure 3. Typical velocity distribution in the rectangular roughness turbulent channel flow.

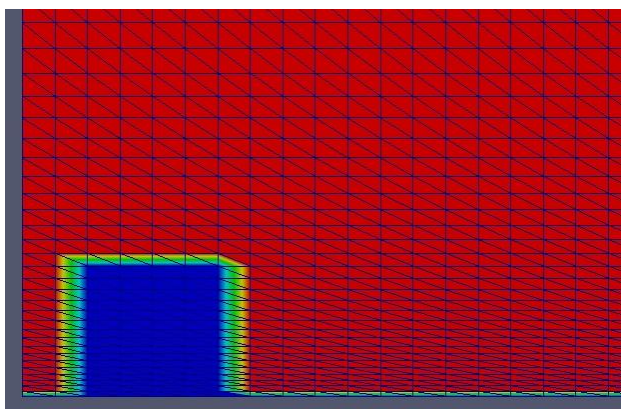

Figure 4. Detailed view of one roughness element with domain grid (the grid is hexahedral, visualization software shows the triangles).

Rough wall channel with hemispherical obstacles

Designing the mesh with hemispherical obstacles proved to be quite challenging since adequate representation of hemispheres by a rectangular grid requires fine grid resolution. The following roughness structure was defined in (Chatzikyriakou, et al., 2011b):

- each hemispherical solid obstacle has a height of h_b equivalent to $y^+ = 10$
- obstacles are located on the wall, spaced at a distance S_b equivalent to $y^+ = 40$
- obstacles are arranged in a square lattice

Since the domain has periodic boundary conditions we need to adjust the boundaries (Table 3) to allow an integer number of roughness elements on the wall in x and z directions. Also, the improved resolution in z direction ($\Delta z^+ = 2.5$ vs. $\Delta z^+ = 7.8$ in rectangular roughness case) substantially increases grid size. Even though we only resolve the hemispherical obstacles with 8 points across diameter, the size of

the structured mesh will reach 992x496x150 = 73.8M hexahedral elements (~300M tetrahedral mesh equivalent). Thus, to keep the computational mesh size in check, it was decided to use half of the domain, split along the symmetry plane between the walls. Thus, the y-direction resolution requirements were cut in half and overall mesh size came down to a reasonable 37.4M elements (Table 3).

Table 3. Hemispherical roughness wall simulation mesh parameters

Direction:	Boundaries:	Number of nodes:	Resolution:
x	0.0 … 6.2h	992	$\Delta x^+ = 2.5$
y	0.0 … 1.0h	76	$\Delta y^+ = 0.5 \ldots 6.5$
z	0.0 … 3.1h	496	$\Delta z^+ = 2.5$

Due to domain size reduction and introduction of a symmetry plane DNS results may change. To evaluate this influence a law of the wall of a smooth case with reduced domain was compared with the full domain size result (Figure 5).

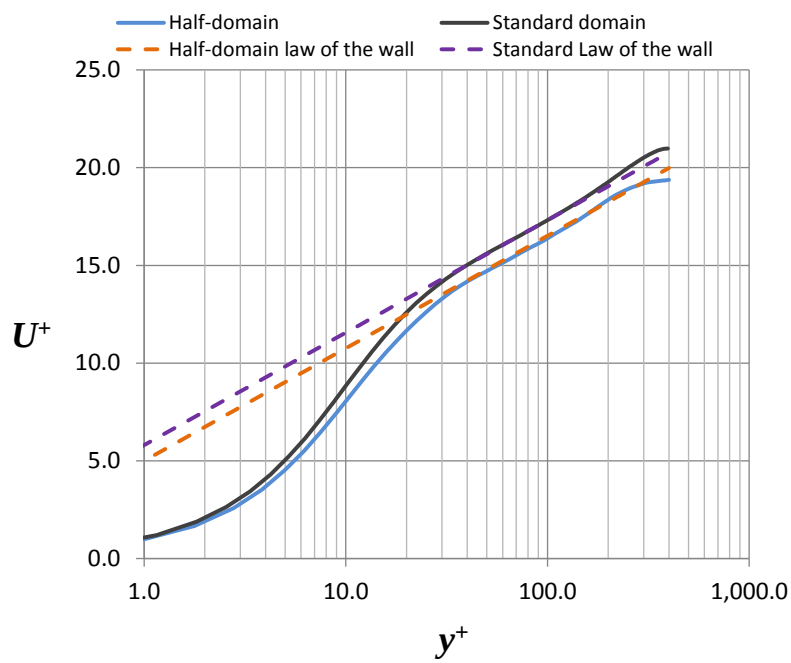

Figure 5. Law of the wall comparison between standard and reduced-size domains with smooth walls.

The law of the wall profile ($U^+ = \frac{1}{\kappa}\ln y^+ + B$) shown in Figure 5 has different parameters in case of reduced size domain (B = 5.0 for reduced-size; B = 5.8 for standard domain. κ = 0.4 in both cases).

Figure 6 shows a typical velocity field in hemispherical roughness reduced-size domain obtained in the presented DNS simulations. Figure 7 demonstrates the level of resolution for each roughness element. In this simulation 1,922 individual hemispherical roughness elements were introduced in a square lattice (62 in x direction by 31 in z direction, Figure 8).

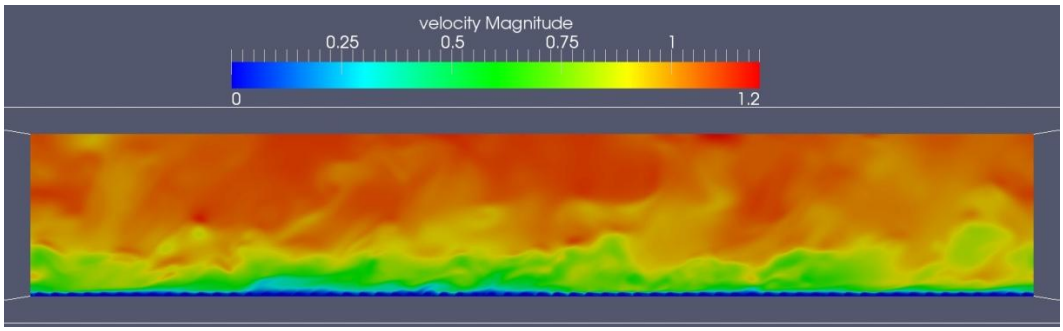

Figure 6. Typical velocity distribution in the hemispherical roughness turbulent channel flow.

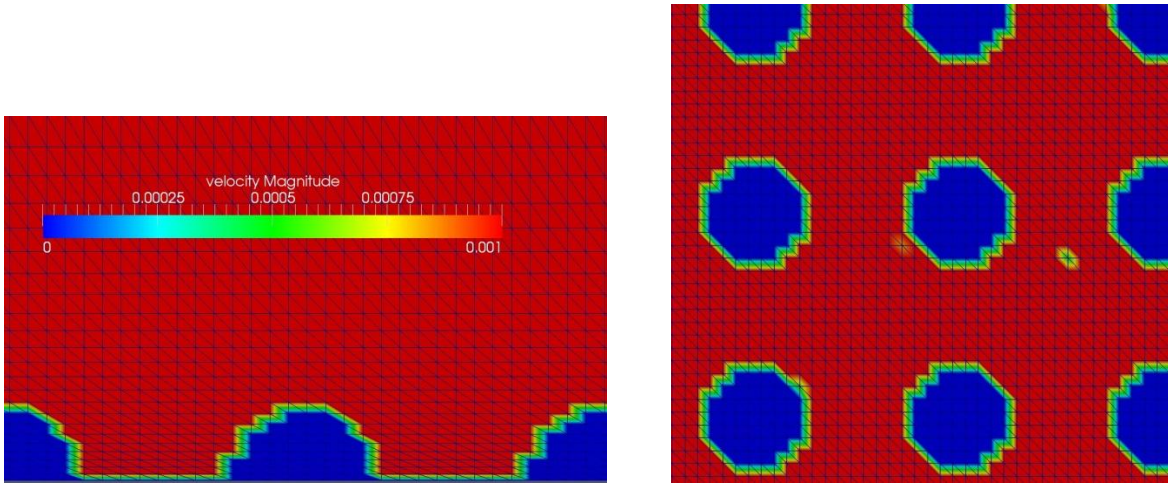

Figure 7. Detailed view of hemispherical roughness elements with computational grid (size view on the left and top view on the right). Blocked regions shown in blue.

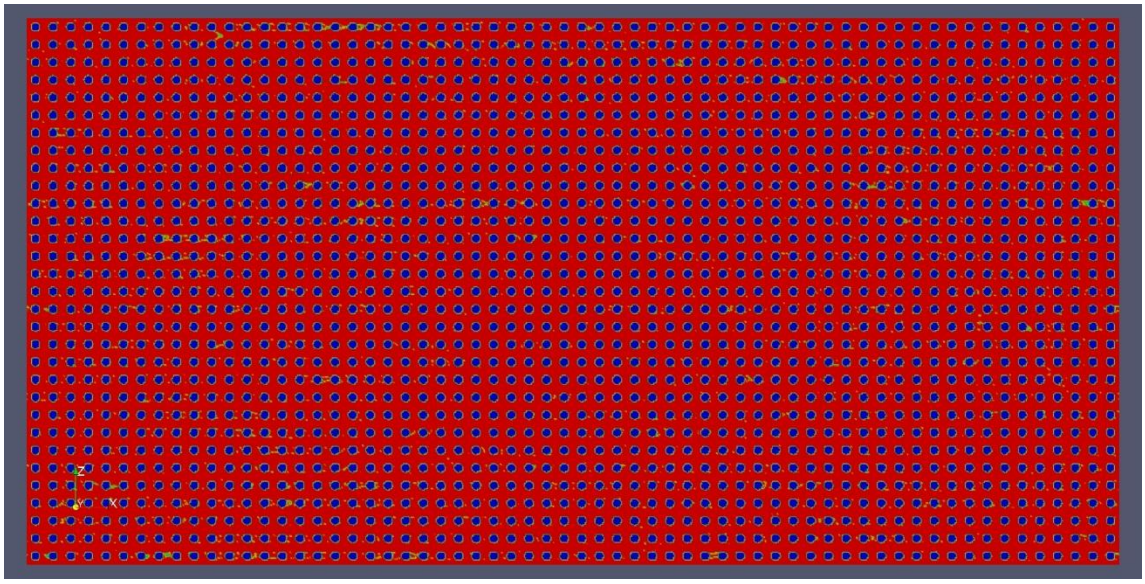

Figure 8. Overview of hemispherical roughness elements.

Results

In this section we will discuss how we collected and processed turbulent statistics and provide comparisons with the available experimental and DNS data.

Data acquisition and analysis

PHASTA has a special feature for collecting flow data via *virtual probes*. These probes can be positioned anywhere in the domain regardless of the actual mesh structure. At the first time step of the simulation each probe location is determined within the finite element mesh and proper weights are computed for quick computation of the velocity, pressure, temperature and other field values at the probe.

Additional pre-processing and post-processing is required to obtain meaningful results. The first step is to generate a list of probes where the velocity field will be recorded. PHASTA uses this list to record time history of flow parameters at each probe. For quality turbulent statistics the number of probes can reach 10 to 15 thousand. We will provide the probe spatial structure for each case under consideration.

The post-processing step entails analyzing the PHASTA virtual probe data. Major turbulence parameters can be determined using the following set of equations:

Mean velocity:

$$U_i^k(t) = \frac{1}{\alpha_k N_e} \sum_{m=1}^{N_e} \left(\frac{1}{N_w} \sum_{j=1}^{N_w} X_k u_m^i \left(t + t_j \right) \right) \tag{3}$$

Turbulent kinetic energy:

$$k^k(t) = \frac{1}{\alpha_k N_e} \sum_{m=1}^{N_e} \left(\frac{1}{N_w} \sum_{j=1}^{N_w} X_k \sum_{i=1}^{3} \tfrac{1}{2} \left(u_m'^i (t + t_j) \right)^2 \right) \tag{4}$$

Turbulent dissipation rate:

$$\varepsilon^k(t) = \nu \frac{1}{\alpha_k N_e} \sum_{m=1}^{N_e} \left(\frac{1}{N_w} \sum_{j=1}^{N_w} \sum_{i=1}^{3} \sum_{k=1}^{3} X_k \left(\frac{\partial u_m'^i (t + t_j)}{\partial x_k} \right)^2 \right) \tag{5}$$

where X_k is the phase indicator function for phase-*k*, $u_m'^i(t+t_j) = u_m^i(t+t_j) - U_i(t)$ is the fluctuation of velocity component-*i* computed during the ensemble run *m* at the time instant $t + t_j$; N_e is the number of ensemble runs, N_w is the number of velocity samples in each window, t is the current time, $t_j = \left(j - N_w/2 \right) \Delta t$ is the local window time, and Δt is the time step.

Smooth wall

Full domain (two walls) smooth wall simulation was performed for 51,500 time steps which corresponds to 17,815 time units (1 time unit: $t^+ = t u_\tau^2/\nu$, t = 821 s). The presented statistics was collected over the last 8,340 time steps (2,970 time units, 137 s), Figure 9.

The mean velocity profile is compared with the law of the wall, Figure 10:

$$U^+ = \frac{1}{\kappa} \ln y^+ + B \tag{6}$$

where κ = 0.4 and B = 5.8. We also show the laminar sublayer law of $U^+ = y^+$, which is expected to be valid for $y^+ < 5$. For comparison purposes, LES results obtained by MIT team are shown as well (Chatzikyriakou, et al., 2011a).

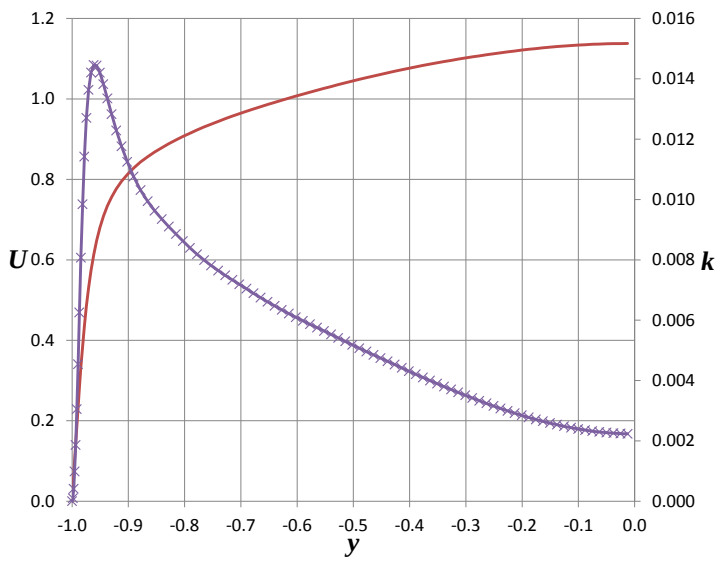

Figure 9. Mean velocity (red line) and turbulent kinetic energy (purple line) profiles for smooth channel flow simulation.

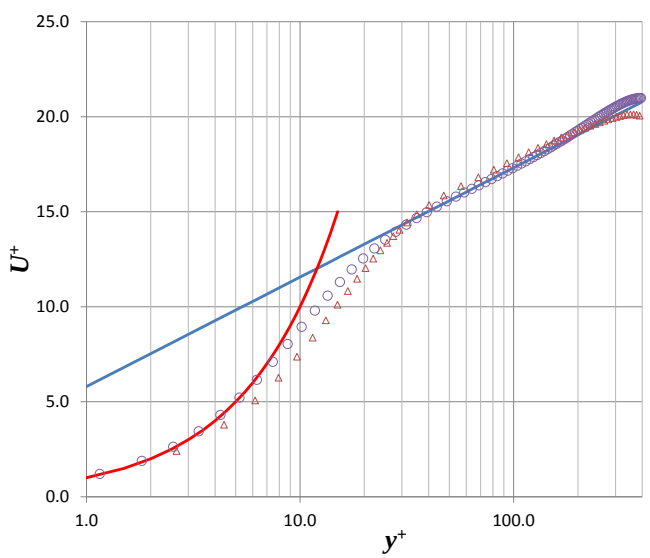

Figure 10. Smooth wall channel flow compared with the law of the wall. PHASTA (circles) and TransAT LES (Chatzikyriakou, et al., 2011a) (triangles) results are shown.

Friction factor

Friction coefficient for the smooth walls simulation can be estimated using:

$$f \equiv 8h\left(-\frac{dp}{dx}\right)\Big/\left(\rho U_m^2\right) \qquad (7)$$

Considering the smooth wall conditions with Re_D = 29,500 (based on hydraulic diameter, corresponds to Re_τ = 400) the Moody's diagram friction factor estimate is 0.024. The obtained DNS based result is f = 0.02419.

More detailed statistics will be considered for the rough wall cases and compared with smooth wall results.

Square rod roughened wall

Full domain (two walls) rough wall simulation was performed for 21,600 time steps which corresponds to 3,840 time units (1 time unit: $t^+ = tu_\tau^2/\nu$, t = 177 s). The presented statistics was collected over the last 4,860 time steps (868 time units, t = 40 s) and was also compared with the next-to-last time windows of the same width to ensure that the solution is converged (Figure 11 last 270 time units are shown in dashed lines and previous time window result is shown in solid lines). *Further runs are underway to ensure better mean velocity turbulent kinetic energy profile convergence*. *Even current results are consistent with the validation data though.*

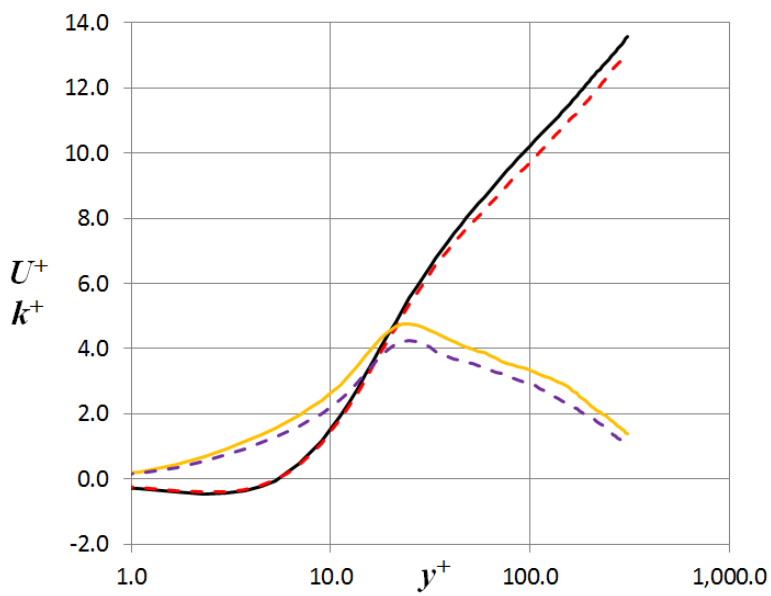

Figure 11. Comparison of mean velocity and turbulent kinetic energy profiles at measurement station 2 averaged at two consecutive time windows to ensure the code statistical convergence for rectangular roughness case. Latest time window is shown with dashed lines.

Four sets of virtual probes were used to record the flow information in this case. The probes' locations were consistent with the measurements of (Ashrafian, et al., 2004). The following locations were used (Figure 12):

- Section 1: x/λ = 0.312
- Section 2: x/λ = 0.71
- Section 3: x/λ = 0.875
- Section 4: x/λ = 1.0

Figure 13 mean velocity profiles at the 4 stations. We can observe a zero velocity at station 4 below the roughness height, as well as backflow at stations 2 and 3 for $y^+ < 6$ and at station 1 at $y^+ < 9$. This is consistent with the picture observed by (Ashrafian, et al., 2004), see Figure 12.

Figure 14 show the mean velocity profiles in various coordinated published by (Ashrafian, et al., 2004) for both rectangular roughness channel and smooth wall channel (Moser, et al., 1999). PHASTA results are consistent and shown in Figure 15.

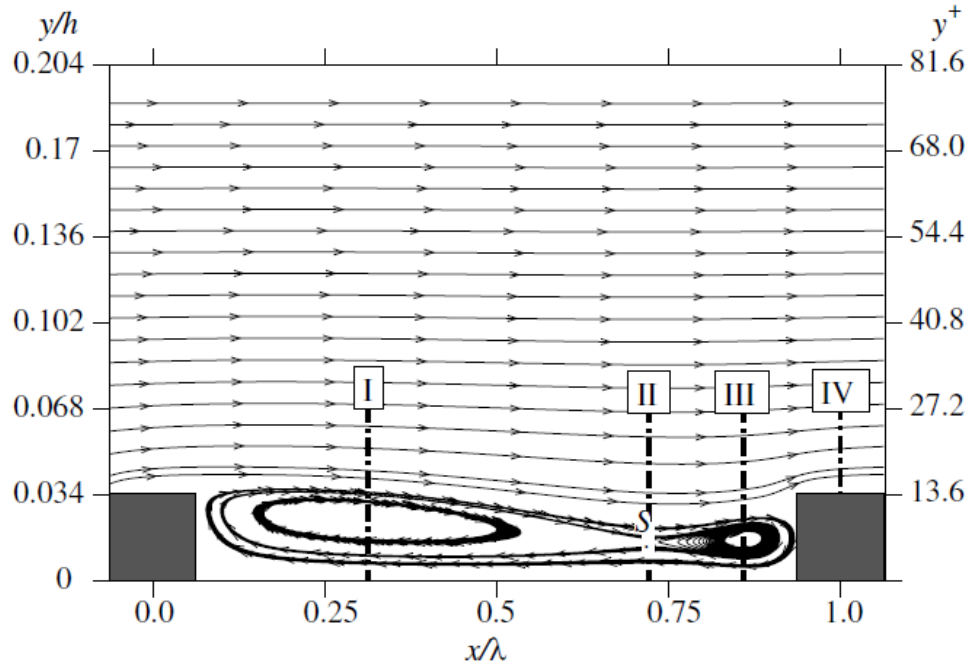

Figure 12. Measuring station locations with respect to rectangular roughness elements (Ashrafian, et al., 2004).

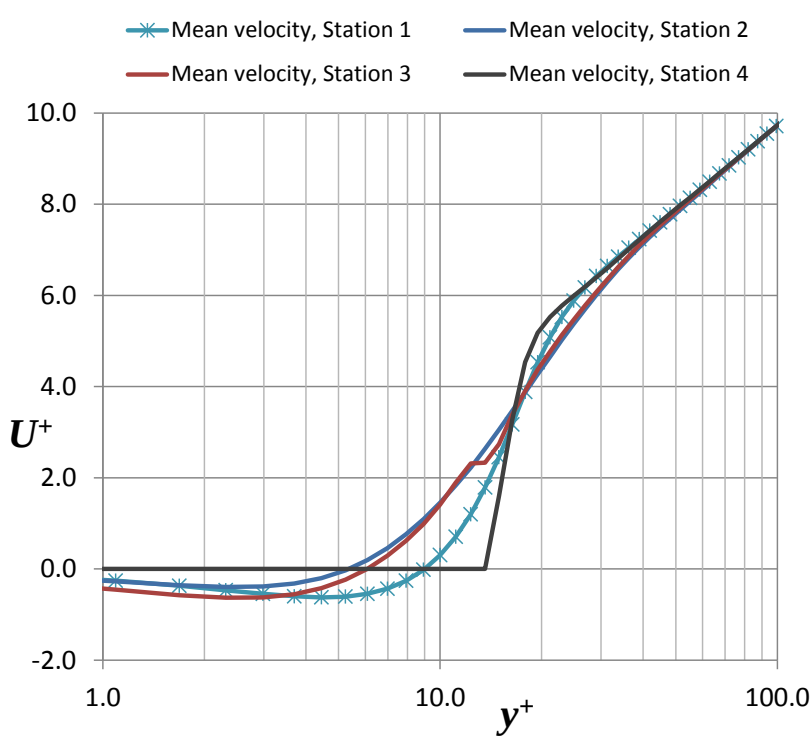

Figure 13. PHASTA results of inner scaling mean velocity profiles at 4 stations shown in Figure 12.

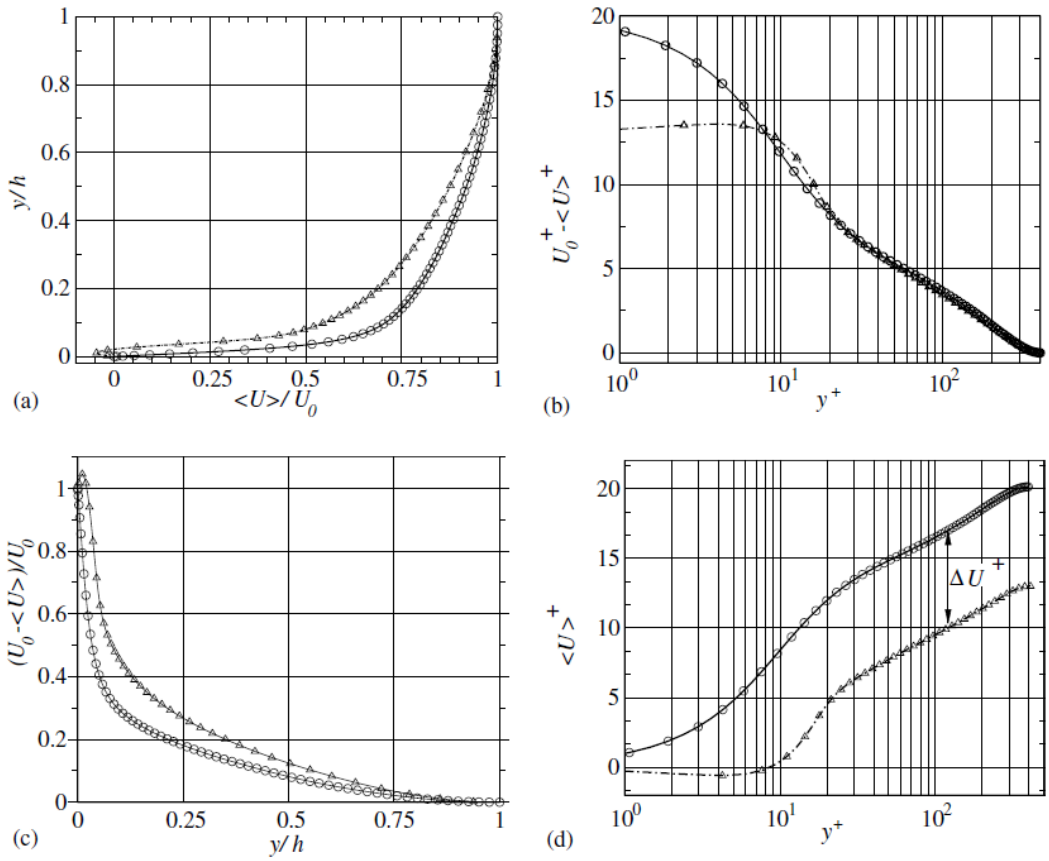

Figure 14. Mean velocity (triangles) profiles at x/λ = 0.312 obtained by (Ashrafian, et al., 2004). Circles show smooth channel data by (Moser, et al., 1999). (a) outer scaling; (b) defect law, inner scaling; (c) defect law, outer scaling and (d) inner scaling. Figure is scanned from (Ashrafian, et al., 2004).

Figure 16 shows the law of the wall plot of PHASTA results for both smooth and rough channels compared with data of (Krogstad, et al., 2005). For a constant pressure gradient used in both simulations we observe a decrease in average velocity due to roughness, as expected. The log-law region is shifted according to the law-of-the-wall:

$$U^+ = \frac{1}{\kappa}\ln y^+ + B - \Delta U^+ \qquad (8)$$

where ΔU^+ is roughness function which quantifies the increase of local drag due to roughness. (Bakken & Krogstad, 2003) suggested the following correlation for the roughness function:

$$\Delta U^+ = \frac{1}{\kappa}\ln k^+ + C \qquad (9)$$

where C = 1.9 for rod-roughened flows. This formula results in estimated value of ΔU^+ = 8.3 for the case under consideration (Ashrafian, et al., 2004). PHASTA results give the value of 7.8 and (Ashrafian, et al., 2004) obtained value of 7.0. Thus, PHASTA provides high quality result.

For comparison purposes we also show the TransAT LES results in Figure 16 (Chatzikyriakou, et al., 2011a).

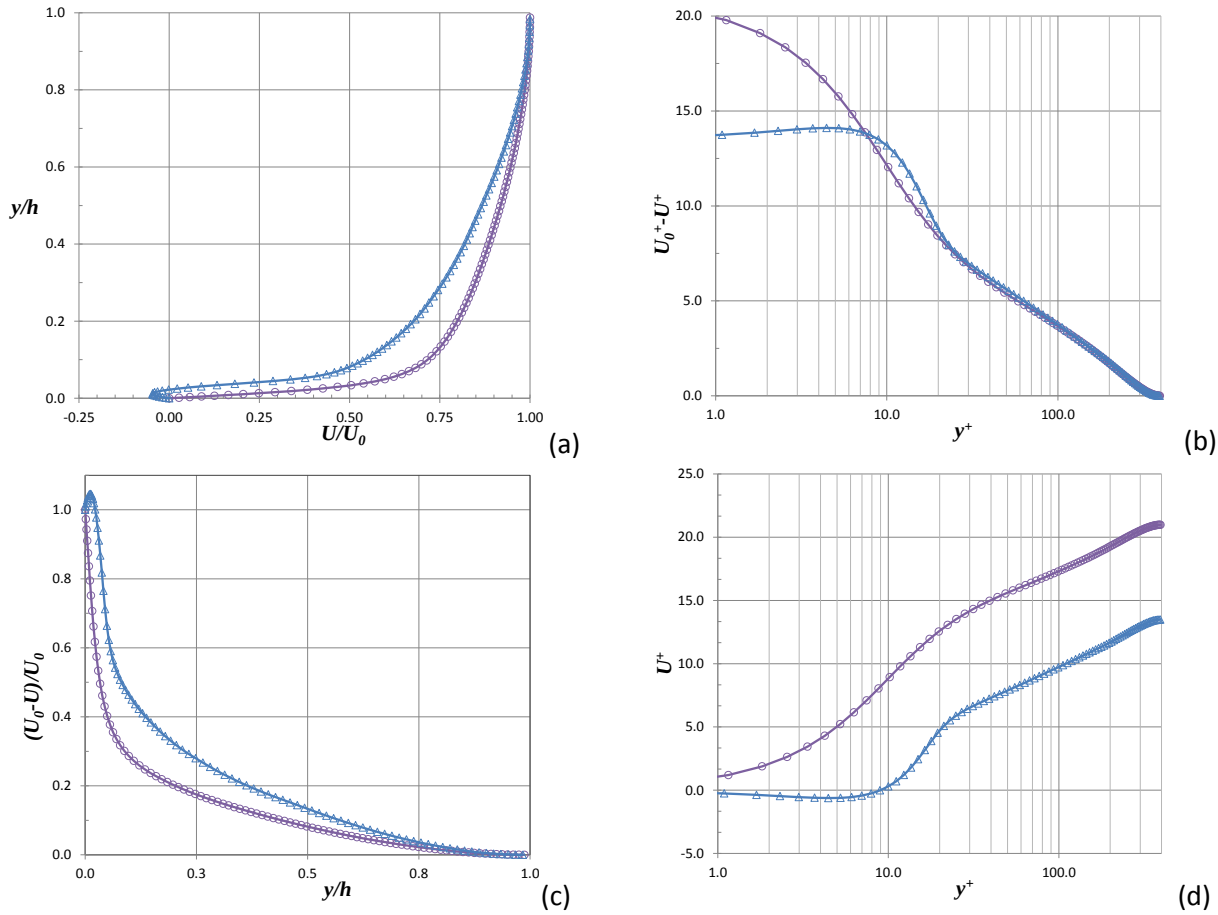

Figure 15. PHASTA mean velocity profiles at x/λ = 0.312 for smooth channel (circles) and rectangular roughness wall channel (triangles). The plots are the same as in Figure 14.

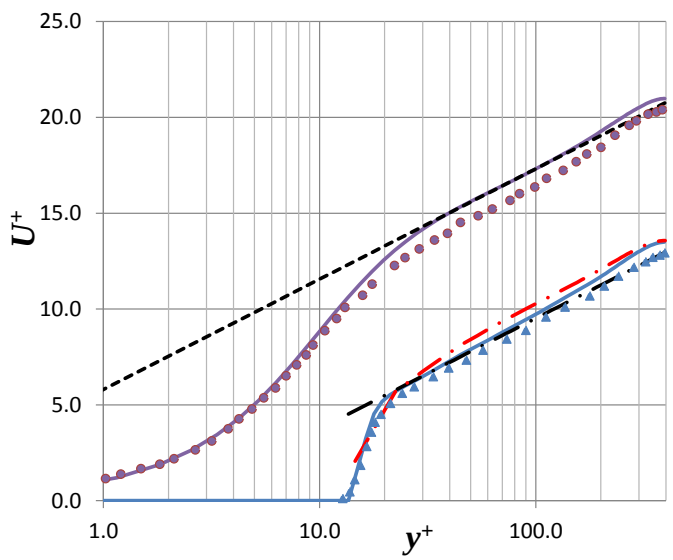

Figure 16. Mean velocity profiles in inner coordinates for smooth and rough (rectangular roughness elements) channel flow simulations by PHASTA (violet and blue solid lines) and DNS results by (Krogstad, et al., 2005) (symbols). TransAT/MIT result is shown in red (Chatzikyriakou, et al., 2011a).

Figure 17 shows the distribution of Reynolds stress components in inner coordinates at different measurement locations. As expected, these functions differ substantially in the near wall region. We overlay the roughness elements height (black solid line) and the estimated thickness of the roughness sublayer (black dashed line) as a 5 times the height (Townsend, 1976). We indeed can observe that all the plotted components converge outside the roughness sublayer into a single curve regardless of the measurement station. Most notable changes occur in the span-wise fluctuation at station 3 which is located in front of the roughness element.

Figure 18 demonstrates the same plots in the outer coordinates and also provides good overview of how roughness thickness and the roughness sublayer relate to the overall channel width.

Friction factor

We'll use Eq. (7) to estimate the friction factor and compare is with Moody's diagram. Considering the rough wall conditions with roughness $\frac{\varepsilon}{d} = 0.0085$; Re_D = 17,000 (based on hydraulic diameter, and computed velocity) the Moody's diagram friction factor estimate is 0.039. The obtained DNS based result is f = 0.071. This result compares very well with the values reported by (Krogstad, et al., 2005): 0.073 for DNS and 0.079 for experiments. This demonstrates that not only the height, but the shape of roughness elements has critical importance on the friction factor.

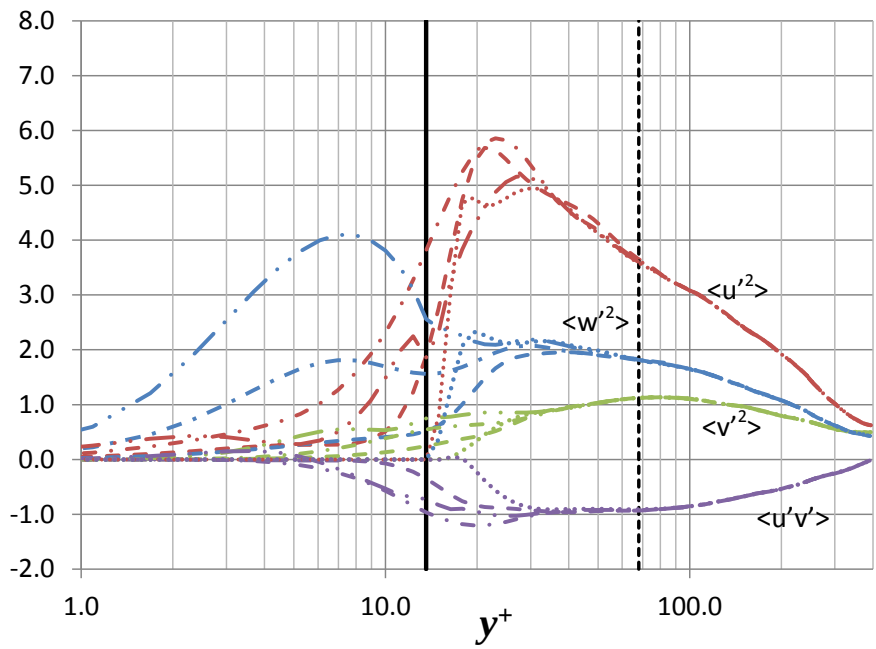

Figure 17. Reynolds stresses in inner coordinates, normalized by u_τ^2. Solid black line shows the height of roughness elements, black dashed line designates roughness sublayer. Colors designate Reynolds stress component: <u'²> is red; <v'²> is green; <w'²> is blue; <u'v'> is violet. Line style shows the measuring station location: Station 1: dashed lines; Station 2: dash-dot lines; Station 3: dash-dot-dot lines; Station 4: dotted lines.

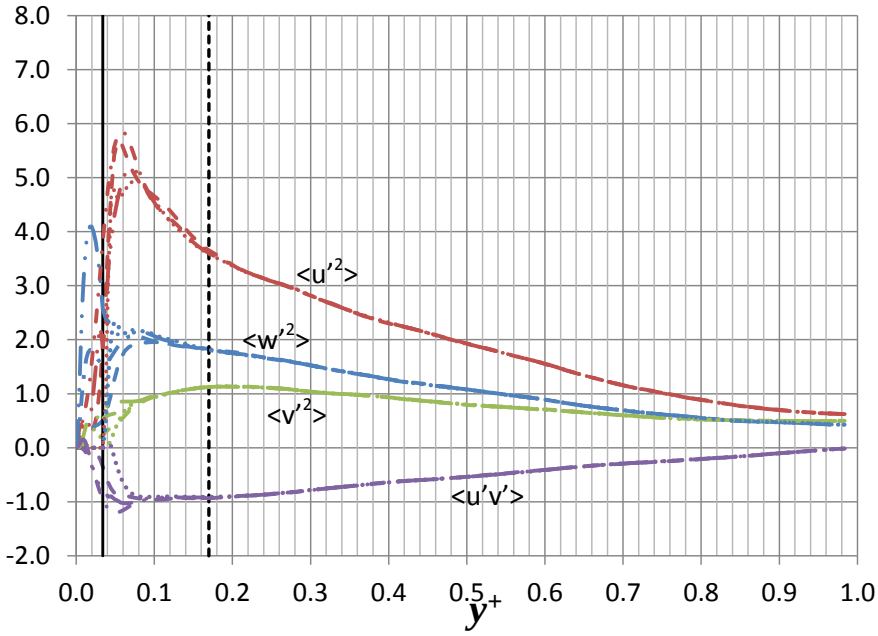

Figure 18. Reynolds stresses in inner coordinates, normalized by u_τ^2. The legend is the same as in Figure 17.

Rough wall channel with hemispherical obstacles

Half domain (wall + symmetry plane) rough wall simulation was performed for 31,000 time steps which corresponds to 3,270 time units (1 time unit: $t^+ = tu_\tau^2/\nu$). The presented statistics was collected over the last 2,420 time steps (270 time units) and was also compared with the next-to-last time windows of the same width to ensure that the solution is converged (Figure 19, last 270 time units are shown in dashed lines and previous time window result is shown in solid lines). *Further runs are underway to ensure better turbulent kinetic energy profile convergence*.

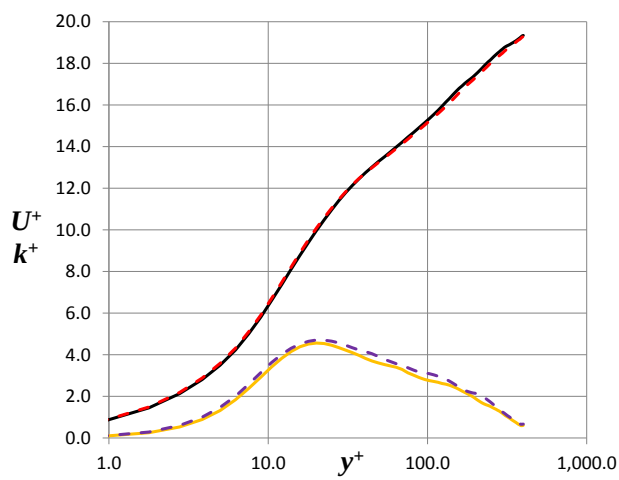

Figure 19. Comparison of mean velocity and turbulent kinetic energy profiles at measurement station 2 averaged at two consecutive time windows to ensure the code statistical convergence for hemispherical roughness case.

In order to analyze the detailed flow behavior around hemispherical obstacles, 7 sets of virtual probes were placed in the computational domain (Figure 20).

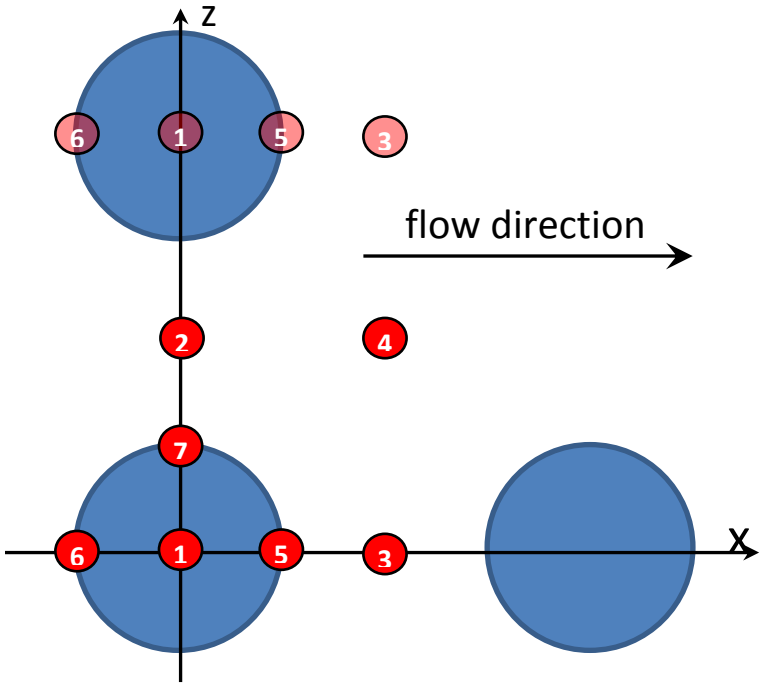

Figure 20. Location of 7 virtual probe sets in the hemispherical roughness case.

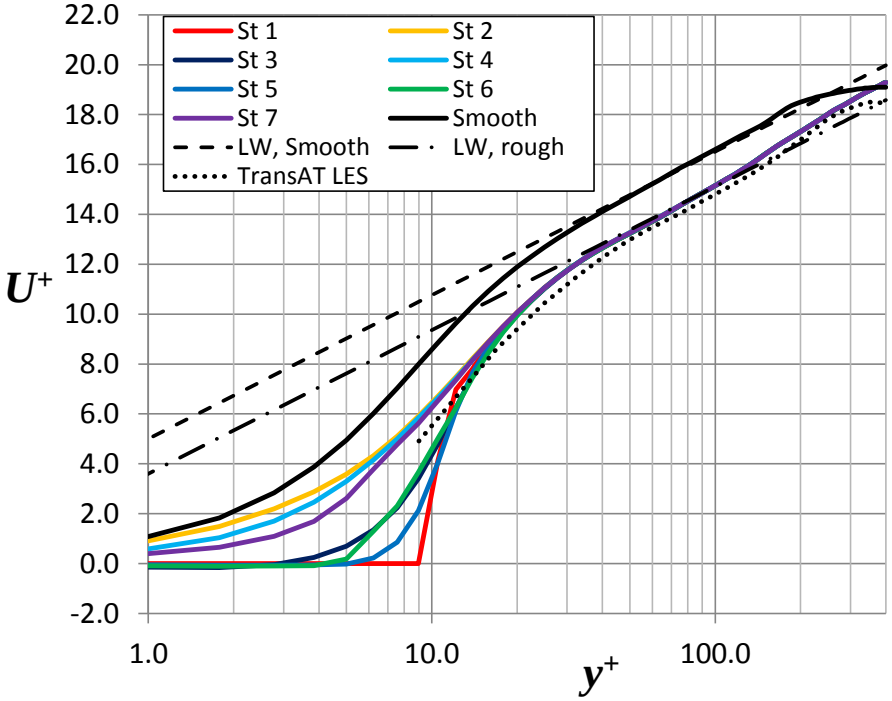

Figure 21. Mean velocity profiles at different measuring stations compared with the smooth wall result and the law of the wall plots. Dotted line shows TransAT LES (Chatzikyriakou, et al., 2011a).

The purpose of this advanced probe placement was to measure and quantify the turbulent quantities in the different locations and provide advanced knowledge for multiphase boiling turbulence model development. For each probe we will provide mean velocity, turbulent kinetic energy and other quantities. We expect to see most of the difference in the region of $y^+ < 30$ (note that the obstacles height is $y^+ = 10$).

Figure 21 shows the set of velocity profiles at each of the 7 probe locations. As expected, the least affected by the presence of the obstacles are probes sets #2, #4 and #7 (see locations in Figure 20) and the probe set #1 is the most affected since it is located normal to the center of each hemispherical obstacle.

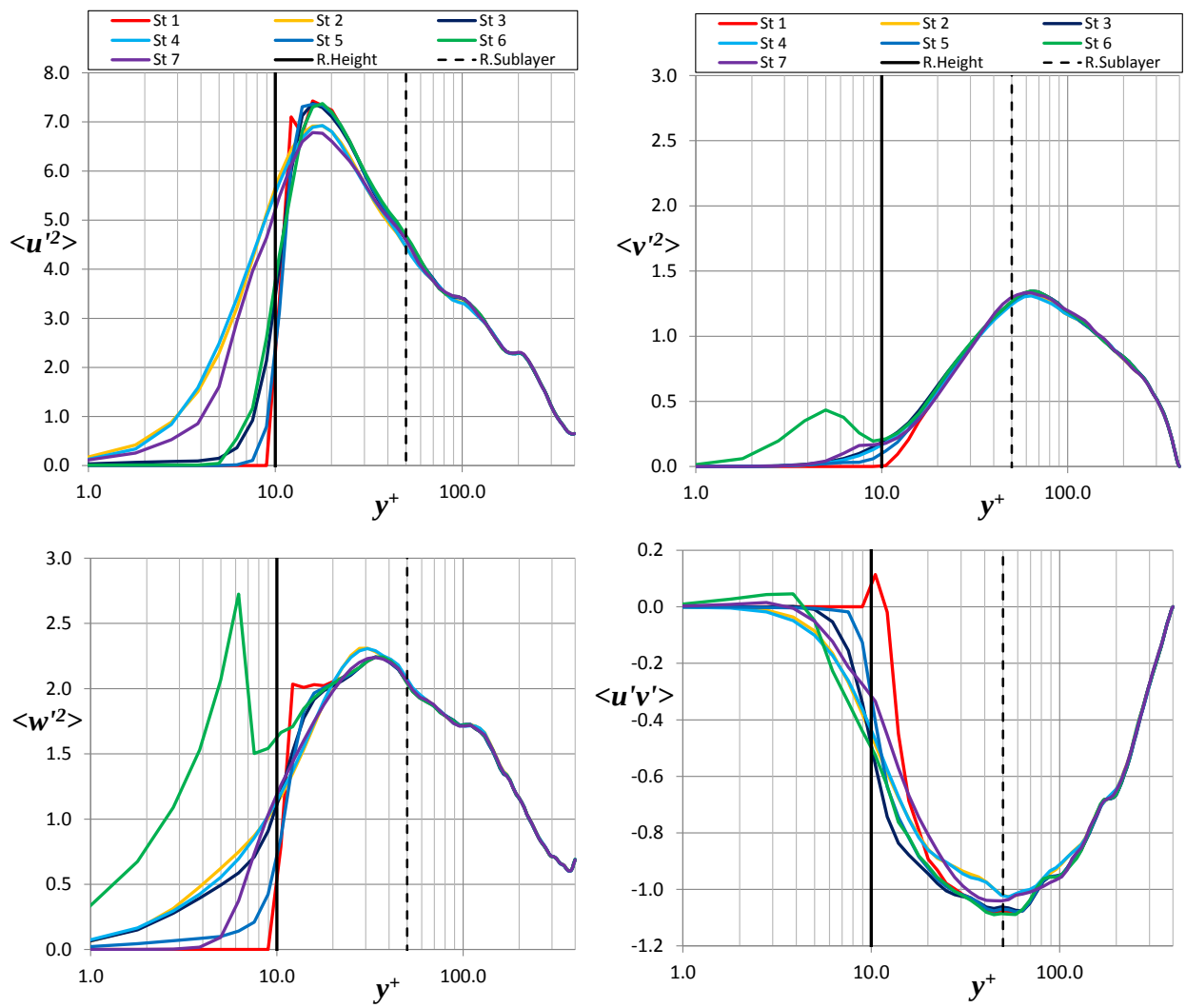

Figure 22. Reynolds stresses in inner coordinates, normalized by u_τ^2. Solid black line shows the height of roughness elements, black dashed line designates roughness sublayer. Each plot shows one component for all 7 measuring stations. Coloring is consistent with Figure 21.

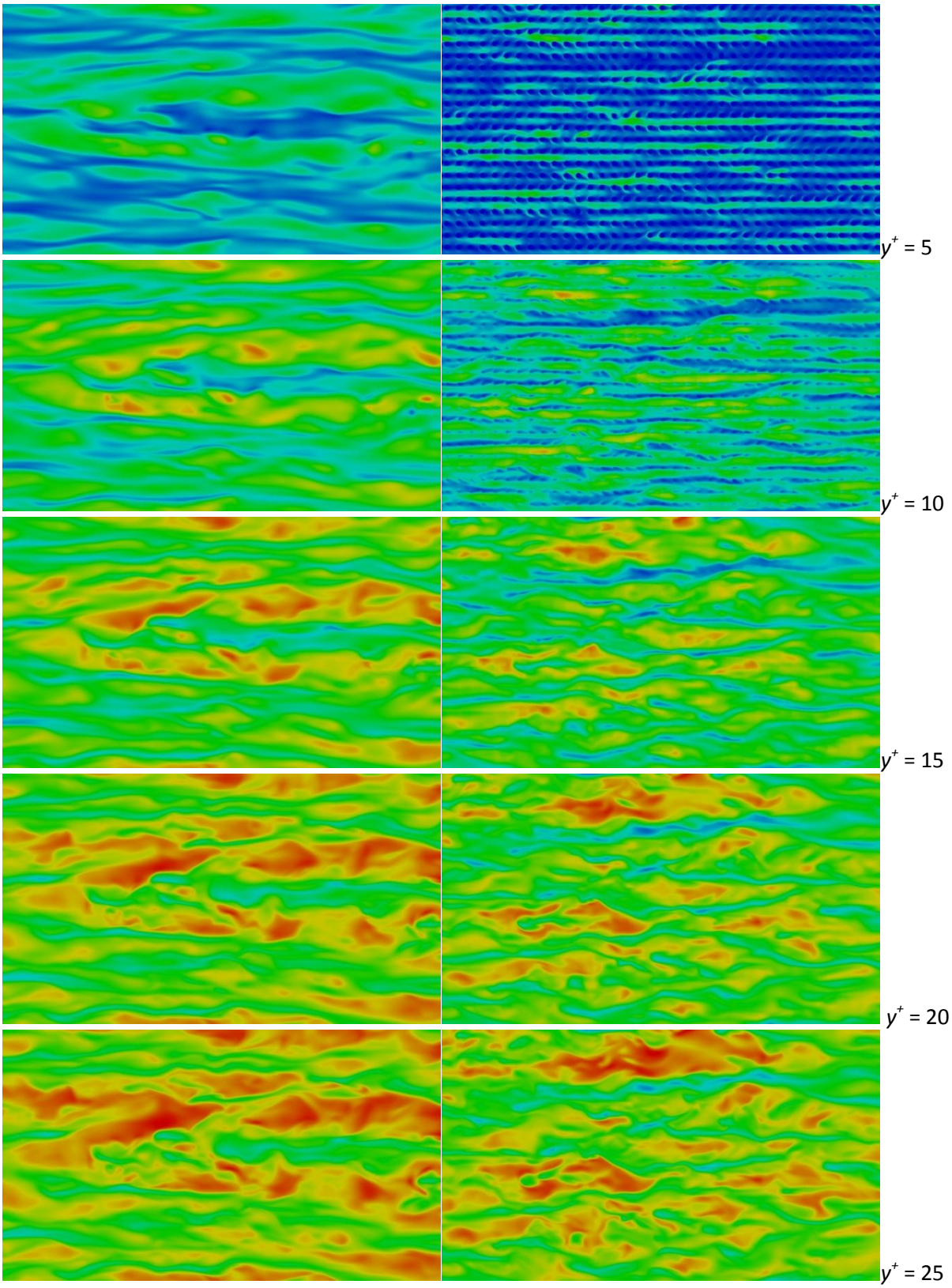

Figure 23. Comparison of velocity magnitude structure in planes, parallel to the wall at various y^+ locations. Smooth wall solution is shown on the left and rough wall with hemispheres on the right.

Figure 22 presents the Reynolds stresses distribution at the 7 measurement stations. We can observe that all of the components mostly converge outsize the roughness sublayer boundary (dashed line). Also, span-wise ($<w'^2>$) and normal-to-the-wall ($<v'^2>$) measurements at station 6 are dramatically different than the other locations. This is the point of flow "impact" on the hemispherical obstacle and thus it's induces a turn in the flow direction. *More data may be required to achieve better statistics*.

Turbulence structures

Figure 23 shows velocity magnitude contours in planes parallel to the wall at various y^+ locations. On the right we can see rough wall results and on the left smooth wall. We can clearly see the effect of the roughness elements at y^+ = 5 and 10, and the different flow structure at y^+ = 15..25 (the biggest structures of the turbulence are smaller in the rough wall flow case).

Friction factor

We'll use Eq. (7) to estimate the friction factor and compare is with Moody's diagram. Considering the rough wall conditions with roughness $\frac{\varepsilon}{d} = 0.00625$; Re_D = 26,000 (based on hydraulic diameter, and computed velocity) the Moody's diagram friction factor estimate is 0.035. The obtained DNS based result is f = 0.0303.

PHASTA **strong** scaling study

A single large bubble turbulent channel flow case has been used to test PHASTA scaling abilities in two-phase flow applications. The problem geometry is shown in Figure 1. The dimensional parameters are provided in Table 4. These parameters were non-dimensionalized for the PHASTA run. Only density/viscosity values were used for the simulation (right column of Table 4).

Table 4. Gas/Liquid properties in the simulation:

Parameter	Dimensional value	Non-dimensional:
Pressure, bar	70	n/a
Liquid	water	n/a
Gas	air	n/a
Temperature, °C	27.0	n/a
Liquid Density, kg/m^3	996.5	1.0
Gas Density, kg/m^3	81.25	0.08128251
Liquid viscosity, kg/m-s	$8.514 \cdot 10^{-4}$	$3.6574 \cdot 10^{-4}$
Gas viscosity, kg/m-s	$1.858 \cdot 10^{-5}$	$7.9918 \cdot 10^{-6}$

A typical velocity field and interface with level set distance field is shown in Figure 24.

In order to perform a strong scaling estimate of two-phase PHASTA runs on Jaguar at a reasonable cost only 20 time steps were performed using the described case on different processor counts. The initial conditions were the same for each run. Those conditions were similar to Figure 24 to represent a more typical load on the code during fully-developed simulations (vs. transients from artificial initial conditions which may be more costly).

To eliminate the costs associated with code initialization computational times for 5 iterations and 15 iterations were recorded. The difference was taken as the time required for 10 iterations (right part of Table 5). Hexahedral mesh with 10.5 M elements was used.

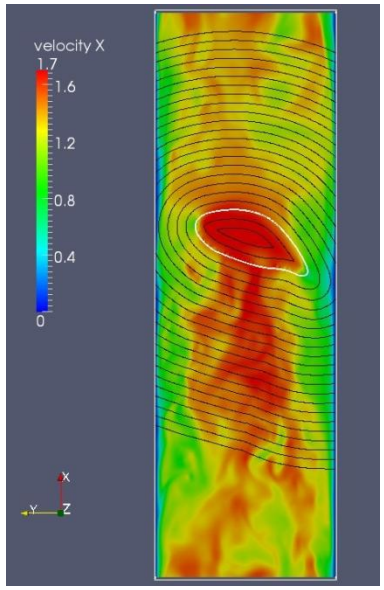

Figure 24. Cross-section of large bubble simulation domain with velocity distribution shown in color, interface (white line) and level set distance field contour (black lines).

From Table 5 one can get an impression that 256-core case gives the most performance. However, provided the wall-clock time savings delivered by higher-core count cases, even 2048 - 4096 cases can be used for the problem under consideration. A substantial increase in performance by going from 64 to 256 cores can be explained by a significant load on each core (164,063 hex elements per core) in the low core count cases. Interestingly, the increase in number of cores from 6144 to 8192 did not produce any wall clock time savings on the 10 iteration basis.

Table 5. Summary of PHASTA strong scaling study

El/proc:	*N cores*	*Total time:*	*Ideal time:*	*%:*	*5 iter time:*	*15 iter time:*	*Diff:*	*Ideal 15-5:*	*%:*
164,063	64	4520.71	4520.71	100%	1281	3404	2123	2123	100%
82,031	128	2012.84	2260.36	112%	583.6	1518	934.4	1061.5	114%
41,016	256	966.89	1130.18	117%	281.2	713.3	432.1	530.75	123%
20,508	512	521.58	565.09	108%	182	405.3	223.3	265.37	119%
10,254	1024	304.18	282.54	93%	123.5	245.3	121.8	132.68	109%
5,127	2048	170.95	141.27	83%	70.74	139.6	68.86	66.34	96%
3,418	3072	161.6	94.18	58%	87.62	141.1	53.48	44.22	83%
2,563	4096	132.39	70.64	53%	113.3	168.4	55.1	33.17	60%
1,709	6144	96.02	47.09	49%	44.36	82.64	38.28	22.11	58%
1,282	8192	97.11	35.32	36%	331.4	369.9	38.5	16.58	43%

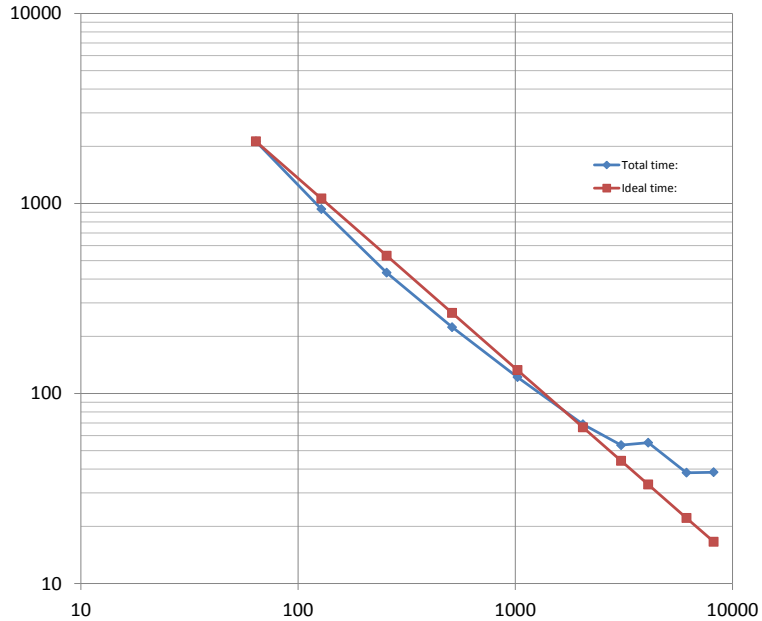

Figure 25. Wall clock time vs. Number of cores. 10 iteration times are shown in seconds.

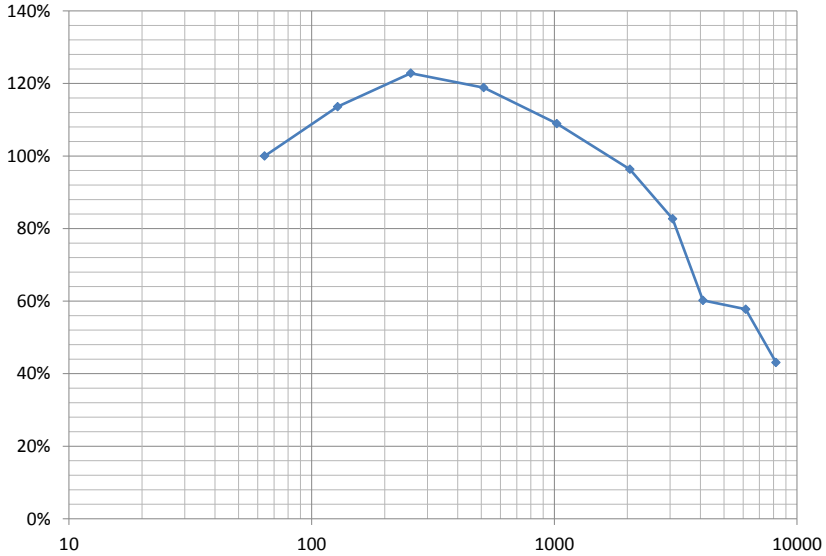

Figure 26. Total time to ideal time ratio. Perfect scaling would mean a horizontal line at 100%.

PHASTA **weak** scaling study

Single-phase PHASTA channel flow runs were used to weak scaling studies. To keep the mesh resolution constant while changing the overall mesh size a different length in stream-wise direction was considered. Table 6 presents the overview of cases considered.

Table 6. Weak scaling study domain parameters (Re_τ = 400)

N cores:	L_x	L_y	L_z	N_x	N_y	N_z	*Mesh size*	*Elem/core:*	Δy^+, *m*
300	2.0	2.0	π	320	150	248	11,904K	39,680	0.0025
600	4.0	2.0	π	640	150	248	23,808K	39,680	0.0025
900	6.0	2.0	π	960	150	248	35,712K	39,680	0.0025
1,200	8.0	2.0	π	1280	150	248	47,616K[1]	39,680	0.0025

In order to test the effect of the output load on the performance, two times were computed for each case. The problems wrote out a restart file every 25 time steps; we have recorded the wall clock time at iteration numbers 10; 29; 49 and 60. This way, T_1 = (Time @ 60 – Time @ 10)/50 will give a good estimate of a performance including output; and T_2 = (Time @ 49 – Time @ 29)/20 will give us a performance without any output operations.

Table 7. Weak scaling PHASTA performance

N cores:	*T@10*	*T@29*	*T@49*	*T@60*	T_1	T_2
300	963.8	3064	5271	6487	110.46	110.35
600	847.2	2550	4314	5288	88.816	88.2
900	961.5	2846	4802	5879	98.35	97.8
1,200	n/a					

Computational cost summary

ORNL leadership computing facility (Jaguar, 2011) was used to perform direct numerical simulations presented in this report. The number of cores used in the simulations varied between 2,004 and 10,080 depending on a particular case and grid size. Overall, about 3.6M CPU-hours were used to perform benchmark simulations (as of 09/25/2011).

Note that availability of supercomputing facility significantly decreased after the summer months which is an expected trend due to ongoing upgrades of the machine as well as other users catching up on their allocations. It would be **beneficial** to align future supercomputing milestone due dates with greater system availability periods (first half of a calendar year) and perform more code development testing in the second half of the year.

Conclusions and Future Work

The presented research demonstrated direct numerical simulation capabilities for single-phase flows with various types of wall roughness. PHASTA solver was used for all presented simulations. The following observations were made:

- DNS can provide a very detailed, reliable information about complex flow structures
- As was expected, DNS runs are very computationally expensive and require a substantial effort just to obtain the raw results.
- Velocity and Reynolds stress profiles obtained from PHASTA are consistent with the available experimental and independently-obtained DNS data

[1] This grid has not been generated due to memory limit using currently available 128G memory machine

- Newly obtained results can be further analyzed to help develop CFD closure laws for roughened wall flows and can help develop boundary condition formulations for CFD of boiling flows.

Any possible future developments within the Benchmark #1 problem formulation must be very well defined in terms of fitting into CASL challenge problems framework. While it may be interesting to see the results for various wall roughness types, it is *essential* to understand the complexity and associated costs of performing DNS simulations.

References

Ashrafian, A., Andersson, H. I. & Manhart, M., 2004. DNS of turbulent flow in a rod-roughened channel. *Heat and Fluid Flow,* Volume 25, pp. 373-383.

Bakken, O. M. & Krogstad, P. A., 2003. *Stress measurements in a rough wall channel flow using a variable angle method of calibration for X-probes.* s.l., s.n., pp. 105-110.

Bolotnov, I. et al., 2011. Detached Direct Numerical Simulation of Turbulent Two-phase Bubbly Channel Flow. *Int. J. Multiphase Flow,* Volume 37, pp. 647-659.

Chatzikyriakou, D., Lakehal, D. & Buongiorno, J., 2011a. *Personal communication,* s.l.: MIT.

Chatzikyriakou, D., Lakehal, D. & Buongiorno, J., 2011b. *Turbulent flow in closed channel with flat walls featuring a pattern of small hemispherical solid obstacles,* s.l.: s.n.

Jaguar, 2011. *National Center for Computational Sciences - Jaguar.* [Online]
Available at: http://www.nccs.gov/computing-resources/jaguar/
[Accessed 19 July 2011].

Jansen, K. E., 1993. Unstructured grid large eddy simulations of wall bounded flows. *Annual Research Briefs, Center for Turbulence Research, NASA Ames/Stanford University,* p. 151.

Jansen, K. E., 1999. A stabilized finite element method for computing turbulence. *Comp. Meth. Appl. Mech. Eng.,* Volume 174, pp. 299-317.

Krogstad, P. A., Andersson, H. I., Bakken, O. M. & Ashrafian, A., 2005. An experimental and numerical study of channel flow with rough walls. *J. Fluid Mech.,* Volume 530, pp. 327-352.

Moser, R., Kim, J. & Mansour, N., 1999. Direct numerical simulation of turbulent channel flow up to Ret = 590. *Phys. Fluids,* Volume 11, pp. 943-945.

Nagrath, S., Jansen, K. E., Lahey, R. T. & Akhatov, I., 2006. Hydrodynamic simulation of air bubble implosion using a FEM based level set approach. *Journal of Computational Physics,* Volume 215, pp. 98-132.

Sahni, O. et al., 2006. Efficient anisotropic adaptive discretization of the cardiovascular system. *Computer Methods in Applied Mechanics and Engineering,* 195(41-43), pp. 5634-5655.

Tejada-Martinez, A. E. & Jansen, K. E., 2005. A parametric-free dynamic subgrid-scale model for large-eddy simulation. *Computer Methods in Applied Mechanics and Engineering,* 194(9), pp. 1225-1248.

Townsend, A. A., 1976. *The structure of turbulent shear flow.* 2nd ed. s.l.:Cambridge University Press.

Trofimova, A. V., Tejada-Martínez, A. E., Jansen, K. E. & Lahey, Jr., R. T., 2009. Direct numerical simulation of turbulent channel flows using a stabilized finite element method. *Computers & Fluids,* Volume 38, pp. 924-938.

Whiting, C. H. & Jansen, K. E., 2001. A stabilized finite element formulation for the incompressible Navier-Stokes equations using a hierarchical basis. *International Journal of Numerical Methods in Fluids,* Volume 35, pp. 93-116.

Zhou, M. et al., 2010. Cardiovascular flow simulation at extreme scale. *Comput. Mech.,* Volume 46, pp. 71-82.